Z. Phys. A – Atomic Nuclei 336, 411–422 (1990)

Zeitschrift für Physik A
Atomic Nuclei

Fission product energies and anisotropies following complete fusion of $^{16}O + ^{238}U$

D.J. Parker [1]*, J.J. Hogan [2], and J. Asher [1]

[1] Nuclear Physics and Instrumentation Division, Harwell Laboratory, Oxfordshire, United Kingdom
[2] Department of Chemistry, McGill University, Montreal, Quebec, Canada

Received December 4, 1989; revised version February 23, 1990

Radioactive recoil techniques have been developed for measuring angular distributions and range distributions of individual fission products following heavy ion induced fission. From these measurements, values can be extracted for the recoil velocity of the fissioning nucleus, the velocity imparted by fission, and the fission anisotropy. These techniques were applied to reactions of 101 MeV ^{16}O on ^{238}U, and confirmed that the reaction mechanism is essentially entirely complete fusion-fission. Accepting this, the data determine the kinetic energy release in forming the various products to a precision of 1%; while the overall magnitude of the energy is in good agreement with previous results, the data suggest a systematic correlation between kinetic energy and the position of a product on the nuclear charge dispersion curve, not previously reported, which is similar to but significantly larger in magnitude than the effect expected from simple Coulomb repulsion. Significant variations in anisotropy are also observed between products, which appear to be partially correlated with the variations in kinetic energy.

PACS: 25.85.Ge

1. Introduction

While the processes of spontaneous fission and thermal neutron induced fission have been extensively studied, and proton induced fission has been studied to energies of hundreds of GeV, much less work has been devoted to investigating details of the fission process resulting from light heavy ion induced reactions, although an understanding of the fission process would seem to be an essential pre-requisite to exploring the mechanisms of reactions on very heavy target nuclei.

More than twenty five years ago, Viola and Sikkeland [1, 2] first studied the occurrence of binary fission in reactions of ^{238}U with light heavy ions at energies up to approximately 10 MeV/u. Essentially all work performed since on fissioning systems has been done with on-line counter techniques measuring the total energy release, gross angular distributions, or, most pertinent to an understanding of the competing mechanisms of interaction, fission fragment angular correlations. At energies only slightly above the Coulomb barrier, several distinct reaction mechanisms may be present; however, the bulk of the fission cross-section occurs following complete fusion, characterized by full momentum transfer to the compound nucleus.

To date, such on-line measurements are unable to resolve the mass and charge of individual fission products. The distributions which are reported are generally summed over several masses, making it very difficult to extract any detailed information about the competing mechanisms.

In contrast, off-line detection of β-decaying fission products enables unique identification of the product mass and charge, although the latter my be complicated by the presence of short-lived β-decay precursors. By collecting the fission products emitted during the reaction in appropriately designed catchers and then measuring the geometric distribution through the catchers for a particular product, the complete velocity distribution may, in principle, be determined. Hence one can investigate the way in which properties such as the fission energy and anisotropy of the angular distribution vary with fragment mass, as well as detect the contribution of mechanisms other than complete fusion to formation of the individual products. Recently, the Seaborg group has carried out recoil studies [3, 4] of 240 MeV ^{12}C on ^{238}U which have largely concentrated on the incomplete fusion-fission processes occurring at 20 MeV/u.

We have developed techniques, described in Sect. II, for measuring both the angular distribution and the projected range distribution of individual fission products.

* Present address: School of Physics and Space Research, University of Birmingham, UK

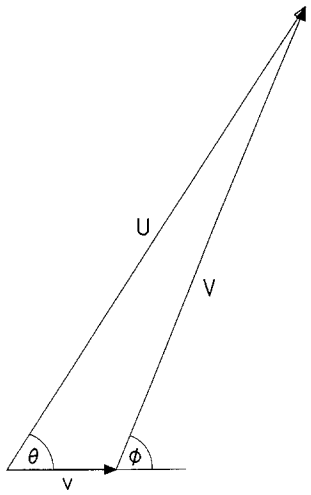

Fig. 1. Kinematics of the fission process. The laboratory velocity of a fission fragment, U, is the vector sum of v and V

From analysis of these two distributions for each detected product, it is possible to extract three principal parameters which characterize the reaction mechanism and the fission process: the recoil velocity, v, of the fissioning system, the additional velocity, V, acquired by the product in the fission process, and the anisotropy, $\omega = P(0°)/P(90°)$, of the fission angular distribution. Figure 1 shows the relationship of v and V; the velocity, U, of the emitted fission fragment in the laboratory frame is the vector sum of v and V. In essence, the forward/backward asymmetry of the measured laboratory angular distribution provides a measure of the ratio v/V, while the maximum range observed in the range distribution is related to the sum, $v+V$; combining the results of the two measurements enables the values of v and V to be deduced. In cases where more than one process populates the given product, the values obtained represent averages over the different processes.

It should be noted that both the experimental techniques and the subsequent analysis represent refinements of methods used in the early years of fission studies, which were reviewed by Alexander [5].

The value of v serves to identify the reaction mechanism prior to fission. Complete fusion is characterized by full momentum transfer, leading to a unique value for the recoil velocity

$$v = v_{cn} = (2 m_p E)^{1/2}/(m_p + m_t)$$

(where m_p and m_t are the masses of the projectile and target and E is the incident laboratory energy). Any other mechanism, such as incomplete fusion or particle transfer, involves reduced momentum transfer and hence a lower value of v.

The values of V and ω reflect details of the fission process itself. V is related to the energy release in fission; however, in order to interpret the meaning of V in detail, it is necessary to correct for the fact that the detected fission product differs from the original emitted fission fragment as a result of neutron evaporation. The anisotropy parameter, ω, is related to the amount of angular momentum deposited in the excited system. For heavy ion induced fission, angular momentum deposition may be considerable and may be expected to modify the fission process significantly. These questions are discussed in Sect. IV.

We have applied these techniques to studying the reactions of 101 MeV ^{16}O on ^{238}U, which are believed on the basis of previous work [2] to proceed almost exclusively via the mechanism of complete fusion, with a view to understanding the fission process in such systems. Sikkeland et al. [2] measured 3.2% of the fission events from 110 MeV ^{16}O on ^{238}U to be non-compound nuclear (NCN), and extrapolating their curve down in energy suggests about 1–2% NCN events at 101 MeV. It should be noted that recent on-line recoil studies [6] of evaporation residues from both light (non-fissile) and heavy (fissile) system have shown that, although incomplete fusion only begins to make a significant contribution as a reaction mechanism at energies well above the Coulomb barrier, it is present at a low level right down to the barrier.

As described in Sect. II, we have measured product yields for approximately forty radioactive fission products; for many of these we have also measured the angular distribution and projected range distribution, and have extracted values for the parameters v, V, and ω as described in Sect. III. The values of v obtained are generally consistent with complete fusion. In Sect. IV we discuss the variation of the observed values of V and ω with product mass and Z. Using a simple model for the neutron multiplicities, which acounts rather well for the measured product yields, we derive the total kinetic energy release associated with formation of each product, and compare this to the variation expected from an elementary calculation of the Coulomb energy. This work appears to be the only study measuring recoil properties as well as yields of a wide range of individual fission products in light heavy ion induced fission at anything like comparable energies.

II. Experimental procedure

Three types of experiment were performed at the Harwell Variable Energy Cyclotron, one to measure the individual fission product yields, a second their angular distributions, and a third, their range distributions. The three recoil experiments differed only in the geometry of their catchers. A beam of 101 MeV $^{16}O^{5+}$ was used, corresponding to an energy far enough above the Coulomb barrier for interaction with ^{238}U to ensure a reasonable fission cross-section. In all cases, individual fission products were identified by off-line γ-ray spectroscopy, and their decays, often complex because of β-decay feeding, were followed over several months.

Two separate fission product yield measurements were performed, concentrating respectively on the short-lived and long-lived products. In each a target comprising 1 mg/cm^2 depleted ^{238}U deposited on aluminum and a 25 μm thick aluminum catcher were mounted inside

Table 1. Cumulative (CUM) and independent (IND) nuclides for which yields were measured, with decay details used. σ_{fwd} is the yield actually detected in the forward hemisphere, σ_t the deduced total yield in both hemispheres, and σ_A the total mass yield evaluated using the charge dispersion curve discussed in the text

Product	CUM/IND	Half-life	γ-ray (keV)	Branching ratio (%)	σ_{fwd} (mb)	σ_t (mb)	σ_A (mb)
^{91}Sr	CUM	9.52 h	556	61.3	3.9±0.1	7.0 ±0.2	7.6±0.2
^{92}Sr	CUM	2.71 h	1384	90.0	3.2±0.1	5.9 ±0.2	6.9±0.2
^{95}Zr	CUM	64.0 d	757	55.4	5.6±0.3	10.1 ±0.5	10.4±0.6
^{96}Nb	IND	23.4 h	778	96.9	0.8±0.07	1.43±0.13	19.0±1.7
^{97}Zr	CUM	17.0 h	658	106.0	5.3±0.1	9.5 ±0.2	11.4±0.2
^{97}Nb(g+m)	IND	72.1 m	658	98.5	1.5±0.3	2.7 ±0.5	18.2±3.7
^{99}Mo	CUM	2.75 d	140	90.7	8.0±0.3	14.3 ±0.5	14.5±0.6
^{103}Ru	CUM	39.3 d	497	89.5	10.1±0.2	18.0 ±0.4	18.1±0.4
^{104}Tc	CUM	18.4 m	358	89.0	8.6±1.4	15.3 ±2.5	17.7±2.9
^{105}Ru	CUM	4.44 h	724	46.7	9.3±0.2	16.5 ±0.3	17.2±0.3
^{107}Rh	CUM	21.7 m	303	66.0	14.1±3.6	25.0 ±6.4	25.7±6.6
^{111}Ag(g+m)	CUM	7.45 d	342	6.68	29.0±3.0	51.2 ±5.3	51.9±5.4
^{112}Pd	CUM	21.1 h	617	50.0	9.4±0.2	16.6 ±0.4	20.8±0.5
^{112}Ag	IND	3.14 h	617	42.5	2.3±0.3	4.1 ±0.5	23.3±3.0
^{113}Ag(g+m)	CUM[a]	5.37 h	298	10.0	12.7±1.0	22.4 ±1.8	24.2±1.9
^{117}Cd(g+m)	CUM[b]	2.40/3.40 h	1303/1066	18.3/23.2	6.9±1.7	12.1 ±3.0	15.5±3.8
^{122}Sb(g+m)	IND	2.70 d	564	70.8	2.5±0.1	4.4 ±0.2	22.7±0.9
^{124}Sb(g+m)	IND[c]	60.2 d	603	98.4	6.0±0.4	10.5 ±0.7	28.1±1.9
^{126}I	IND	13.0 d	389	32.2	1.2±0.2	2.0 ±0.3	17.4±2.6
^{127}Sb	CUM	3.85 d	686	35.3	3.7±0.4	6.4 ±0.7	17.8±2.0
^{129}Sb	CUM	4.32 h	813	43.5	1.1±0.2	2.0 ±0.3	17.6±2.8
^{130}I(g+m)	IND[d]	12.4 h	536	99.0	4.9±0.1	8.5 ±0.2	21.2±0.4
^{131}I	CUM	8.02 d	365	81.2	7.3±0.1	12.7 ±0.2	24.7±0.4
^{132}Te	CUM	3.26 d	773	78.7	2.8±0.1	4.9 ±0.2	65.9±2.4
^{132}I(g)	IND[e]	2.30 h	773	76.4	3.5±0.2	6.1 ±0.4	22.3±1.3
^{132}Cs	IND	6.48 d	668	97.4	1.5±0.2	2.6 ±0.4	12.2±1.6
^{133}I(g+m)	CUM	20.8 h	530	87.0	4.0±0.1	6.9 ±0.2	33.9±0.9
^{135}I	CUM	6.61 h	1260	28.6	2.3±0.2	4.0 ±0.4	86.6±7.5
^{135}Xe(g+m)	IND	9.08 h	250	90.4	2.4±0.2	4.1 ±0.4	19.1±1.7
^{136}Cs	IND	13.2 d	819	99.7	3.4±0.1	5.9 ±0.2	16.7±0.5
^{140}Ba	CUM	12.8 d	487	52.9	3.7±0.1	6.4 ±0.2	25.5±0.7
^{140}La	IND	40.3 h	487	45.9	3.2±0.1	5.5 ±0.2	13.8±0.4
^{141}Ce	CUM	32.5 d	145	48.4	9.4±0.5	16.1 ±0.9	19.2±1.1
^{142}La	CUM	1.52 h	641	47.4	3.4±0.3	5.8 ±0.6	18.5±1.6
^{143}Ce	CUM	33.0 h	293	42.8	5.8±0.2	9.9 ±0.3	17.9±0.6
^{147}Nd	CUM	11.0 d	91	27.9	5.3±0.4	9.1 ±0.7	12.9±1.0
^{150}Pm	IND	2.68 h	334	69.0	2.5±0.4	4.3 ±0.7	10.9±1.7
^{153}Sm	CUM	46.7 h	103	28.3	4.4±0.4	7.5 ±0.7	14.3±1.3

[a] Excludes 20% of isomeric state
[b] Ground state and isomeric state determined separately and summed
[c] Excludes 20% of $M1$ isomeric state
[d] Excludes 17% of isomeric state
[e] No sign of isomeric state

an electrically-suppressed Faraday cup and irradiated at a beam current of approximately 60 particle nA. In the short-lived measurement, the duration of the irradiation was only 20 min, whereas in the long-lived measurement the irradiation lasted 6 h. In each case, after irradiation the target and catcher were counted together 75 mm from the face of a 25% efficient Ge(Li) detector which had previously been calibrated to better than 5% in efficiency and about 0.1% in energy. A continuous sequence of counts was performed over a period of two months. Subsequently, a version of the GAMANAL [7] code was used to find and integrate all peaks and to correct for detector efficiency. For each γ-ray of interest, decay curve analysis was used to confirm the identity of the fission product; half lives and branching ratios were taken from the GSI compilation [8] and are listed in Table 1. The spectra and decay curves were exceedingly complex, due both to the number of fission products and the activated products from the aluminum catcher foil, as well as to β-decay from the charge dispersion. The target thickness (measured using Rutherford backscattering with a 2 MeV α beam to an accuracy of 5%) and the beam fluence (known to an estimated 5%) were then applied to convert the yields to absolute cross-sections, σ_{fwd}, for production of these products in the forward hemisphere. Results are listed in Table 1; the uncertainties do not include the systematic 7% uncertainty in normalization. The knowledge gained of the decay characteristics of each γ-ray line was used in the decay curve analyses of the following experiments. The nuclides

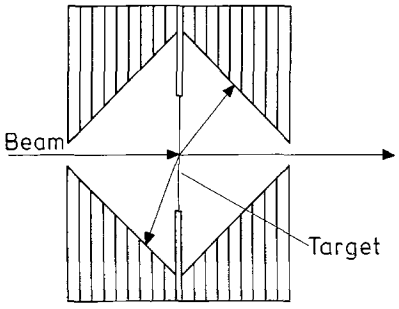

Fig. 2. Cross sectional view of the catcher assembly used for measuring angular distributions. The assembly is cylindrically symmetric about the beam axis

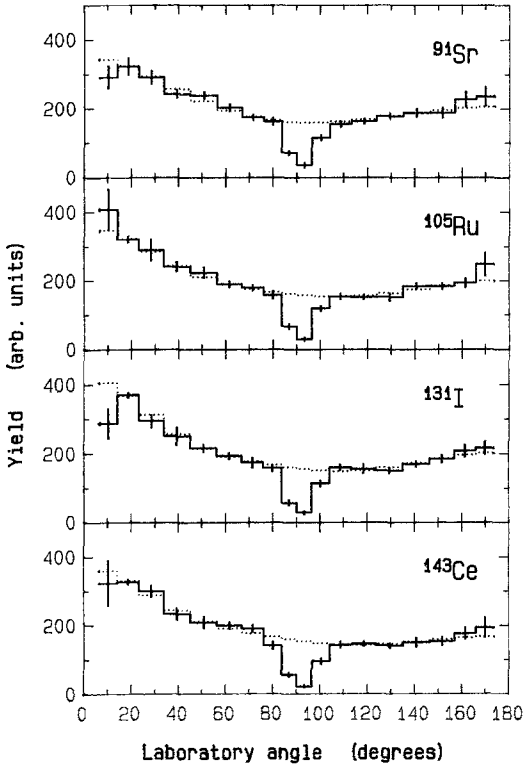

Fig. 3. Measured laboratory angular distributions for four products (solid histograms). The dotted histograms show the fits obtained using a center of mass angular distribution of the form $a+b\cos^2\phi+c\cos^4\phi$

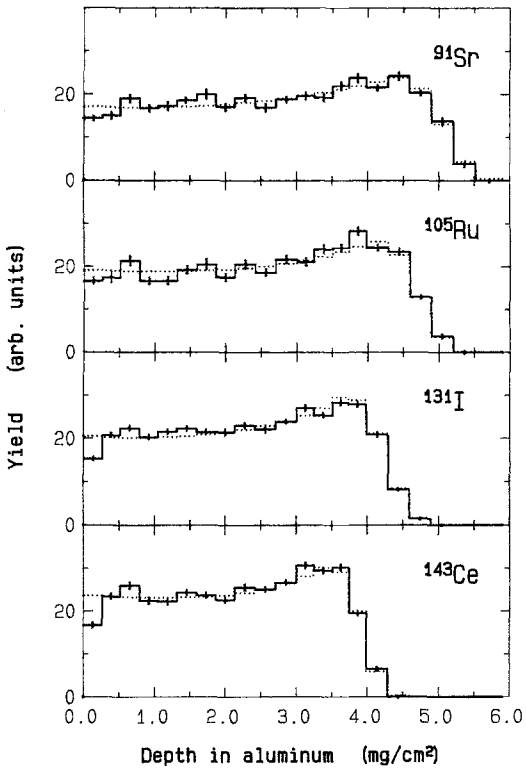

Fig. 4. Measured projected range distributions for the same four products as in Fig. 3 (solid histograms). The dotted histograms show the result of fitting, using the angular distribution previously determined

listed are only those which could reasonably be regarded as either independent yields (IND) or fully cumulative yields incorporating all β-decay precursors (CUM).

The catcher arrangement for the angular distributions, shown in Fig. 2, sandwiched the target (which consisted of 100 μg/cm^2 ^{238}U on 100 μg/cm^2 Al) between eighteen 2 mm thick aluminum plates (nine in the forward direction, nine backward) with a conical hole of half angle 45° machined through each set. A 4 mm diameter hole at each end allowed entrance and exit of the beam, which was collimated to 2 mm diameter. This assembly was irradiated for 14 h at a beam current of 40 particle nA. Afterwards, each ring with fission products captured on the inner bevelled edge was counted repeatedly on the face of one of two 25% efficient Ge(Li) detectors over a period of two months. Spectra were analyzed and decay curve analysis performed for each catcher, as above. A correction factor was applied to normalize the two detector efficiencies at each energy of interest. Finally the angular distribution was obtained by dividing the measured yield in each catcher by the calculated solid angle subtended. Four typical angular distributions are shown in Fig. 3; in each case, the data has been normalized to the same total yield. The angular distributions peak at (or near) 0° and 180°; they are not symmetric in the laboratory frame, being displaced toward forward angles due to the motion of the fissioning system. While the overall acceptance angle for fission products is from 6.3° to 173.7°, accounting for more than 99% of the total solid angle, many of those fission fragments emitted at lab angles near 90° were stopped in the target assemply. This is seen as a reduction in yield in three catchers around 90°; these were excluded from the subsequent analysis.

The third experiment measured fission product differential range distributions, projected along the beam axis, using the conventional stacked foil technique of our previous work [9, 10]. The target comprised 100 μg/cm^2 depleted ^{238}U on a support of 100 μg/cm^2 Al, mounted with the uranium layer downstream; the catcher stack consisted of 25 aluminum foils averaging 200 μgm/cm^2 in thickness. The exact thickness of each foil was measured prior to use by measuring the energy loss in tra-

versing the foil of 5.8 MeV α-particles from a ^{244}Cm source. The target and catcher foils were irradiated for 14 h at a beam current of approximately 35 particle nA. Once again, each catcher foil was repeatedly counted on one of the two Ge(Li) detectors, spectra were analyzed, decay curve analysis performed and the factor to correct the relative efficiencies of the two detectors applied, as above. Finally the range distribution was obtained by dividing the measured yield in each catcher by the thickness of the catcher. Typical range distributions are shown in Fig. 4 for four products. For each product, a continuous distribution of ranges is observed due to the fission angular distribution, with the yield in the first catcher arising from fragments emitted just forward of 90° in the laboratory frame, and the maximum range corresponding to emission at 0°; this maximum range decreases significantly as a function of product mass.

III. Analysis of results

The interdependence of the analysis of the three experiments to determine v, V, ω, and cross-sections dictates the order of discussion of the results below.

A. Angular distributions

In the moving frame of the fissioning nucleus, the fission angular distribution is necessarily symmetric about 90°, and peaks at (or near) 0° and 180°. We represent this by the functional form:

$$\frac{d\sigma}{d\Omega} = a + b\cos^2\phi + c\cos^2\phi$$

where ϕ is the centre of mass angle, or, in terms of the anisotropy ω,

$$\frac{d\sigma}{d\Omega} = a\{1 + (\omega - 1)[\delta\cos^2\phi + (1-\delta)\cos^4\phi]\}$$

where $b/a = (\omega - 1)\delta$ and $c/a = (\omega - 1)(1-\delta)$. The angular distribution observed in the laboratory frame is displaced towards forward angles due to the velocity v of the fissioning nucleus. Since the laboratory angle, θ, is given by the relation $\cot\theta = \cot\phi + k/\sin\phi$, where $k = v/V$ (Fig. 1), the degree of displacement depends only on the ratio k. The yield caught by a catcher plate spanning the laboratory angle from θ_1 to θ_2 is just:

$$2\pi a \int_{\phi(\theta_1,k)}^{\phi(\theta_2,k)} \{1 + (\omega-1)[\delta\cos^2\phi + (1-\delta)\cos^4\phi]\}\sin\phi\, d\phi$$

Least squares fitting of this expression to the measured laboratory angular distribution thus enabled the four parameters a, ω, δ, and k to be determined. Note that $\frac{d\sigma}{d\Omega}(0°) = a\omega$, and $\frac{d\sigma}{d\Omega}(90°) = a$, so that a is simply a nor-

Table 2. Nuclides for which recoil properties were measured. The experimental quantities are k, ω and U_{max}; from k and U_{max} the values of v and V are derived; V_{cf} is an improved estimate of V assuming the complete fusion mechanism. E_k is the experimental estimate of total kinetic energy release, determined from V_{cf} as described in the text (corrected for the difference in range/energy relations), while E_{Coul} is the same quantity predicted on a simple Coulomb basis

Product	CUM/IND	k	ω	U_{max} [a]	v [a]	V [a]	V_{cf} [a]	E_k (Mev)	E_{Coul} (MeV)
^{91}Sr	CUM	0.131±0.015	1.73±0.05	1.762±0.008	0.204±0.024	1.558±0.022	1.538±0.008	171.4±1.9	186.4
^{92}Sr	CUM	0.164±0.027	1.93±0.10	1.734±0.007	0.244±0.041	1.490±0.035	1.510±0.007	169.4±1.7	187.0
^{97}Zr	CUM	0.139±0.011	1.79±0.04	1.691±0.012	0.206±0.017	1.485±0.019	1.467±0.012	174.5±3.0	190.8
^{99}Mo	CUM	0.137±0.010	1.94±0.04	1.686±0.004	0.203±0.015	1.483±0.014	1.462±0.004	175.6±1.0	192.5
^{99}Tc	IND	0.165±0.042	1.84±0.18	1.724±0.007	0.244±0.063	1.480±0.054	1.500±0.007	192.2±1.8	196.1
^{103}Ru	CUM	0.158±0.018	1.68±0.06	1.680±0.004	0.229±0.026	1.451±0.023	1.456±0.004	185.1±1.1	194.9
^{105}Ru	CUM	0.144±0.008	1.72±0.03	1.634±0.005	0.206±0.012	1.428±0.011	1.410±0.005	182.6±1.4	195.7
^{111}Pd^{m}	IND	0.178±0.041	2.41±0.16	1.582±0.010	0.239±0.056	1.343±0.048	1.358±0.010	192.5±2.9	198.7
^{112}Pd	CUM	0.193±0.014	2.24±0.06	1.547±0.008	0.250±0.018	1.297±0.017	1.323±0.008	183.1±2.3	198.1
^{112}Ag	IND	0.232±0.044	2.31±0.17	1.551±0.009	0.292±0.056	1.259±0.046	1.327±0.009	186.8±2.6	199.3
^{113}Ag	CUM	0.164±0.015	2.25±0.06	1.563±0.007	0.220±0.020	1.343±0.019	1.339±0.007	189.1±2.1	198.6
^{115}Cd	CUM	0.158±0.012	2.05±0.05	1.559±0.007	0.213±0.016	1.346±0.016	1.335±0.007	193.8±2.1	199.1
^{122}Sb	IND	0.186±0.028	2.10±0.12	1.447±0.005	0.227±0.035	1.220±0.030	1.223±0.005	186.9±1.6	199.9
^{124}Sb	IND	0.104±0.064	2.15±0.18	1.464±0.008	0.140±0.085	1.324±0.077	1.240±0.008	198.5±2.6	199.9
^{126}Sb	CUM	0.100±0.024	1.85±0.15	[b]					
^{130}I	IND	0.126±0.010	1.74±0.03	1.412±0.006	0.158±0.013	1.254±0.012	1.188±0.006	201.0±2.1	199.3
^{131}I	CUM	0.181±0.009	1.91±0.03	1.410±0.006	0.216±0.011	1.194±0.011	1.186±0.006	202.4±2.1	199.5
^{132}I	IND	0.136±0.031	1.50±0.13	[b]					
^{133}I	CUM	0.207±0.012	1.53±0.04	1.382±0.011	0.237±0.014	1.145±0.016	1.158±0.011	200.1±3.5	199.4
^{135}Xe	CUM	0.163±0.019	1.75±0.08	1.349±0.003	0.189±0.022	1.160±0.019	1.125±0.003	195.7±1.1	198.7
^{136}Cs	IND	0.190±0.035	2.11±0.19	1.346±0.008	0.215±0.040	1.131±0.035	1.122±0.008	197.9±2.9	198.0
^{140}Ba	CUM	0.100±0.036	1.56±0.12	1.328±0.005	0.121±0.044	1.207±0.040	1.104±0.005	204.1±1.9	197.4
^{140}La	IND	0.179±0.017	1.69±0.07	1.316±0.006	0.200±0.019	1.116±0.017	1.092±0.006	200.3±2.2	196.1
^{141}Ce	CUM	0.208±0.024	1.94±0.10	1.306±0.007	0.225±0.026	1.081±0.023	1.082±0.007	197.4±2.6	195.9
^{143}Ce	CUM	0.197±0.012	1.64±0.04	1.299±0.006	0.214±0.013	1.085±0.013	1.075±0.006	202.8±2.3	195.3

[a] $[MeV/u]^{1/2}$

[b] No range distribution measured

malisation constant, ω is the anisotropy, and the parameter δ determines the relative weights of the $\cos^2\phi$ and $\cos^4\phi$ terms.

As discussed in the previous section, data from three catchers around 90° are invalid because products emitted at these angles are stopped in the target; these data were excluded from the fitting process. In general, the data from the first and last catcher plates, which subtend very small solid angles and suffer from a background of activation products due to scattered beam, are of poorer quality than the rest. The fitting procedure was applied twice, once including these data and once without; the results obtained with these data included have been used except where the resulting fit is significantly worse than without them. Effectively then, the four parameters were determined by fitting 13 to 15 data points.

The dotted histograms in Fig. 3 show the fits obtained. The values for the parameters k and ω are listed in Table 2 for all the products for which angular distributions could be measured; it can be seen that these parameters were in general determined to an uncertainty of approximately 10%, though in some cases, where decay curve analysis was particularly difficult or yields were low, the uncertainty is significantly larger. The uncertainty in the determination of δ was large and we do not attach any significance to the values obtained (the parameter a has no significance since the data were arbitrarily normalized).

In order to determine the sensitivity of the ratio k to the algebraic form of the distribution chosen, the data were also analyzed by two other procedures: (*i*) an alternative functional form $a+b\cos^2\phi+c/\sin\phi$ was fitted to the data, and (*ii*) a simple integration procedure was used to determine the midpoint of the distribution in the moving centre-of-mass frame of reference. Both approaches yielded results for the ratio v/V consistent with those listed in Table 2 but with somewhat larger uncertainties. These methods suffered, however, from an inability to define a simple anisotropy, $P(0°)/P(90°)$. It must be stressed that no simple formulation of the angular distribution really fits the yield near 0° and 180° and the form chosen in this work merely allows convenient definition of the desired ratio, v/V, while providing reasonable fits to the data. There is no evidence that the particular formulation has more or less theoretical validity than other approaches.

B. Cross-sections

For the centre of mass angular distribution,

$$\frac{d\sigma}{d\Omega}=a\{1+(\omega-1)[\delta\cos^2\phi+(1-\delta)\cos^4\phi\,]\}$$

it is straightforward to show that the fraction of the yield emitted forward in the laboratory frame is:

$$F_{fwd}=\frac{1+k+\frac{1}{3}(\omega-1)\delta(1+k^3)+\frac{1}{5}(\omega-1)(1-\delta)(1+k^5)}{2[1+\frac{1}{3}(\omega-1)\delta+\frac{1}{5}(\omega-1)(1-\delta)]}$$

The parameters, k, ω, and δ, determined by fitting to the measured laboratory angular distributions as described in the previous section, were used to calculate F_{fwd} for each product for which an angular distribution had been measured, and the results were used to convert the measured cross-sections, σ_{fwd}, for production of nuclides in the forward hemisphere, into total cross sections, $\sigma_t=\sigma_{fwd}/F_{fwd}$, for each nuclide. Since cross-sections were measured for many more nuclides than the 25 nuclides listed in Table 2 for which it was possible to measure angular distributions, interpolated values were used. When plotted against product mass, the values of F_{fwd} which could be extracted were found to lie on a straight line, varying from 0.555 at mass 90 up to 0.582 at mass 140 (the uncertainty in F_{fwd}, which is dominated by the uncertainty in k, was typically 1%, and essentially all values were consistent with this line to within the experimental uncertainty). Accordingly this linear relation has been used to calculate the values of σ_t listed in Table 1; it is believed that the additional uncertainty introduced by the conversion from σ_{fwd} to σ_t is negligible.

C. Range distributions

The principal aim of analyzing the projected range distributions is to determine the quantity $U_{max}=v+V$ from the "endpoint" of the distribution. The exact shape of the distribution (typical examples are shown in Fig. 4) depends upon the angular distribution. In fact, it is interesting to note that in terms of the projected velocity, $U\cos\theta$, the yield distribution has exactly the same form as the center of mass angular distribution, centered at $U\cos\theta=v$. The measured projected range distribution is somewhat distorted because (*i*) the range is not exactly linearly proportional to velocity, and (*ii*) range straggling broadens it.

The measured distributions were fitted, using the values of the parameters already determined for k and the form of the angular distribution, and using a parameterized form of the range/energy relations of Northcliffe and Schilling [11] to convert velocity to range in aluminum. In addition to an arbitrary normalization factor, two fitting parameters were used: U_{max} and a parameter controlling the width of a Gaussian broadening which was superimposed on the velocity in an attempt to reproduce the effect of straggling; this second parameter consistently took a value of approximately 5% of U_{max}. If the fission process responsible for forming a given product involves a distribution of kinetic energies, this will also contribute to the broadening of the measured distribution. A further smearing was applied to account for the finite thickness of the ^{238}U target: recoiling products were assumed to originate with equal probability anywhere between 0 and 0.1 mg/cm^2 before the start of the catcher stack.

The dotted histograms in Fig. 4 show the result of this fitting, which is quite satisfactory. The fitting procedure determines U_{max} to an uncertainty of typically 0.5%, but this precision must be viewed with some caution since spurious results would be obtained if the yield in the last significant catcher were not detected for any

reason. There is also significant systematic uncertainty in the absolute values obtained, due to uncertainty in the range/energy relation used. For cumulative products, a small error is introduced by the use of the range/energy curve for the observed nuclide instead of that for the actual product. These points are discussed further below. The values obtained for U_{max} are listed in Table 2. Like all velocities referred to in this paper, these are in units $[\text{MeV/u}]^{1/2}$. (A velocity of 1 $[\text{MeV/u}]^{1/2}$ corresponds to a value of $\beta = \frac{V}{c}$ of approximately 0.033.)

D. *Results: the reaction mechanism*

From the values of $k = v/V$ determined from the measured angular distribution and $U_{max} = v + V$ determined from the range distribution, it is possible to extract values for the two velocities of interest: $V = U_{max}/(1+k)$ and $v = k\,U_{max}/(1+k)$ for each observed product. The resulting values are listed in Table 2.

The values obtained for v, the recoil velocity of the fissioning nucleus, are plotted in Fig. 5 as a function of product mass. With two exceptions, ^{130}I and ^{140}Ba, all the experimental values are consistent with the theoretical recoil velocity, $v_{cn} = 0.224\ [\text{MeV/u}]^{1/2}$, of the ^{254}Fm compound nucleus formed in complete fusion, which is denoted by the horizontal line in this figure. Quantitatively, the weighted average of the experimental values is $0.96 \pm 0.02\ v_{cn}$ (or 0.94 if the ^{130}I and ^{140}Ba values are included, but these are clearly inconsistent with the assumption of identical v for all products). The present data thus confirm the conclusion of previous work [2] that at this incident energy the reaction mechanism prior to fission is essentially exclusively complete fusion.

It seems likely that the barely significant overall 4% difference in absolute value between the experimental v and the theoretical v_{cn} arises from some systematic effect in the measurements or the analysis. The most likely source of systematic error is the range/energy relations used; the observed discrepancy would arise if the tabulated range values of Northcliffe and Schilling [11] were systematically too high by approximately 4% in this regime, which is quite credible. In this case, all of the velocities determined in the present work would be systematically underestimated by 4% and energies underestimated by 8%; however, as discussed in the next section, there is no evidence of this in the values obtained for the fission energy, which are in good agreement with the values expected from systematics. Although we cannot entirely exclude the possibility that the observed 4% discrepancy arises from a small contribution of mechanisms other than complete fusion, involving smaller recoil velocities, there is no sign of the type of systematic variation between different products expected in that case.

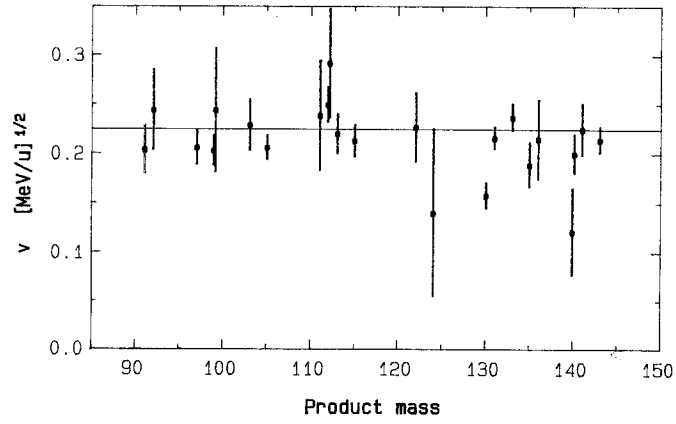

Fig. 5. Experimental values of v, the recoil velocity of the fissioning nucleus; the value v_{cn} expected from complete fusion is shown by the horizontal line

There is no apparent reason why the mechanism responsible for forming the products ^{130}I and ^{140}Ba should be different from that populating all the other products. We conclude, therefore, that the data for these two products are probably incorrect, though we have been unable to locate any errors. It is in the nature of radiochemical studies that occasional points are invalid for no obvious reason, and undue importance should not be attached to isolated experimental values which conflict with the overall trend.

For the remainder of this paper, we shall accept that all of the observed products are formed purely by complete fusion, and attempt to obtain insight into the subsequent fission process. In addition to the production cross-sections, the parameters which contain useful information are the anisotropy, ω, and the fission velocity, V. In the next section we consider the variations in the kinetic energy (derived from V) and the angular anisotropy. Since there is a larger uncertainty in the experimental values of V (arising from the uncertainty in the determination of k) than in the quantity $U_{max} = v + V$ which has been determined with great precision, we shall work from the experimental U_{max} values and, following the assumption that we are dealing with complete fusion, obtain an improved estimate of V as $V_{cf} = U_{max} - v_{cn}$. The values obtained for V_{cf} are listed in Table 2.

IV. Discussion – the fission process

In attempting to interpret the observed data in the context of a model of the fission process, a complication arises in that the observed products are not the primary fission fragments, but are formed from these after evaporation of several neutrons (and in many cases after several β decays). Before any comparison can be made, the extent of this neutron evaporation must be established. Also, since most of the measured data are for cumulative partial chain yields, modelled quantities must be appropriately averaged over the chain of fragments contributing to each observed product. It is therefore necessary to establish the fission charge dispersion curve for each product mass. We approach these questions via consideration of the measured mass yields.

A. Mass yields

Ideally, in order to extract details of the fission yield distribution, it is desirable to have yield values for a number of isobars, so that the center and width of the charge dispersion curve (which is assumed to be Gaussian in form at these energies [12]) can be determined. Alternatively, if independent yields can be extracted for several isotopes of a particular element, the mass dispersion can be determined. The ratio of the width of the mass dispersion curve to that of the charge dispersion curve at any point in the fission product distribution is approximately $\frac{A}{Z}$ where A and Z are the mass and charge of the fissioning nucleus [13].

Unfortunately, in the present experiment it was not possible to determine yields for sufficient nuclides of the same mass to fit any charge dispersion curves (the only mass for which the yields of more than two isobars are known is 132 and the ^{132}Te, ^{132}I, and ^{132}Cs cross-sections are insufficient without knowledge of the yield of ^{132}Xe). In only one case, iodine, was it possible to extract a crude mass dispersion curve using the independent yields of ^{126}I, ^{130}I, and ^{132}I; this appears to be centred around mass 130 and to have a FWHM value of approximately 6 masses.

We have therefore based our initial values for the charge dispersion width and the extent of neutron evaporation on existing data from similar systems, and have investigated the effect of varying these parameters by using them to extract total mass yields from our data, bearing in mind that the mass yield curve should be smoothly varying and symmetric with respect to interchange of a pair of fragments.

Our picture of the fission process is as follows. Starting with the compound nucleus (atomic number Z_{cn}, mass number A_{cn}) we assume that on average ν_{pre} neutrons are evaporated prior to fission, and a further ν_{post} neutrons are evaporated from the pair of fragments after scission, so that in forming the final pair of fission products a total of $\nu = \nu_{\text{pre}} + \nu_{\text{post}}$ neutrons is evaporated from the system. From comparison of the neutron energy spectra measured at 0° and 90°, Hinde et al. [14] have determined the separate yields ν_{pre} and ν_{post} as a function of excitation energy for various heavy ion systems. Further, in the case of ^{19}F + ^{232}Th [15], they investigated the dependence of these quantities on the mass of the observed product, and found, as expected from naive models, that at moderate excitation energy, ν_{pre} is independent of product mass for a given fissioning system, and ν_{post} is approximately proportional to product mass (expected if the excitation energy of the scissioning system is shared between the fragments in proportion to their masses).

Then if scission of the system $(Z_{cn}, A_{cn} - \nu_{\text{pre}})$ gives rise to a fragment of mass A_f it is expected to evaporate, on average, $\frac{A_f \nu_{\text{post}}}{A_{cn} - \nu_{\text{pre}}}$ neutrons. Thus, given a product of mass A_{prod}, the most probable fragment mass A_f leading to formation of this product can be deduced from the relation

$$A_{\text{prod}} = A_f - \frac{A_f \nu_{\text{post}}}{A_{cn} - \nu_{\text{pre}}} \tag{1}$$

We further assume that fission of the ^{254}Fm compound nucleus, which has an excitation energy of 56.3 MeV, can be described by the unchanged charge distribution (UCD) hypothesis [16], so that the most probable charge, Z_p, for a fragment of mass A_f is $\frac{A_f Z_{cn}}{A_{cn} - \nu_{\text{pre}}}$.

Combining these expressions, we find that the most probable charge leading to a final product of mass A_{prod} is

$$Z_p = \frac{A_{\text{prod}}}{A_{cn} - \nu} Z_{cn} \tag{2}$$

We further assume that the standard deviation, S, of the Gaussian charge dispersion curve is independent of mass.

The parameters required to model the effects of neutron evaporation are thus S, ν_{pre} and ν_{post}. Actually, since ν_{pre} and ν_{post} do not appear separately in (2) but only as their sum ν, only this quantity is required at this stage in the modelling.

The results of Hinde et al. [15] for 105 MeV ^{19}F on ^{232}Th give $\nu = 9$ (of which $\nu_{\text{pre}} = 3$ and $\nu_{\text{post}} = 6$), and we have adopted these values as the starting point for our modelling. The value to be used for S, the width of the charge dispersion curve is less well determined. In their recent study of 240 MeV ^{12}C on ^{238}U, Yu et al. [4] found that the iodine yields could be divided into two regions, of which the more neutron deficient isotopes, apparently formed by fissions following central collisions, are most analogous to the products of fusion-fission observed in the present work; this group was observed by Yu et al. to have a mass dispersion curve with FWHM 5.4 mass units. In a radiochemical study of yields from reactions of 222–272 MeV ^{76}Ge on ^{170}Er, which produces the compound nucleus ^{246}Fm with excitation energies of 35–65 MeV, Lützenkirchen et al. [17] found that a FWHM of 5 mass units best fitted the measured yields of near symmetric ($40 \leqq Z \leqq 60$) fragmentation products. Accordingly we took as our initial value $S = 0.9$, corresponding to a FWHM in the mass dispersion curve of 5.2 u.

The following procedure was used to extrapolate the total mass yield, σ_A, for a given product mass from the experimental product yield σ_t. The probability of a fragment of mass A_f having nuclear charge Z' is

$$g(Z', A_f) = \frac{1}{\sqrt{2\pi}S} \int_{Z'-\frac{1}{2}}^{Z'+\frac{1}{2}} \exp -\left(\frac{z - Z_p}{2S^2}\right)^2 \mathrm{d}z.$$

So for an independent product, the fraction of the total mass yield populating the observed product, $\frac{\sigma_t}{\sigma_A}$, is just equal to $g(Z_{\text{prod}}, A_f)$, while for a cumulative product $\frac{\sigma_t}{\sigma_A} = \sum_{Z' \leqq Z_{\text{prod}}} g(Z', A_f)$. ($A_f$ is related to A_{prod} as in

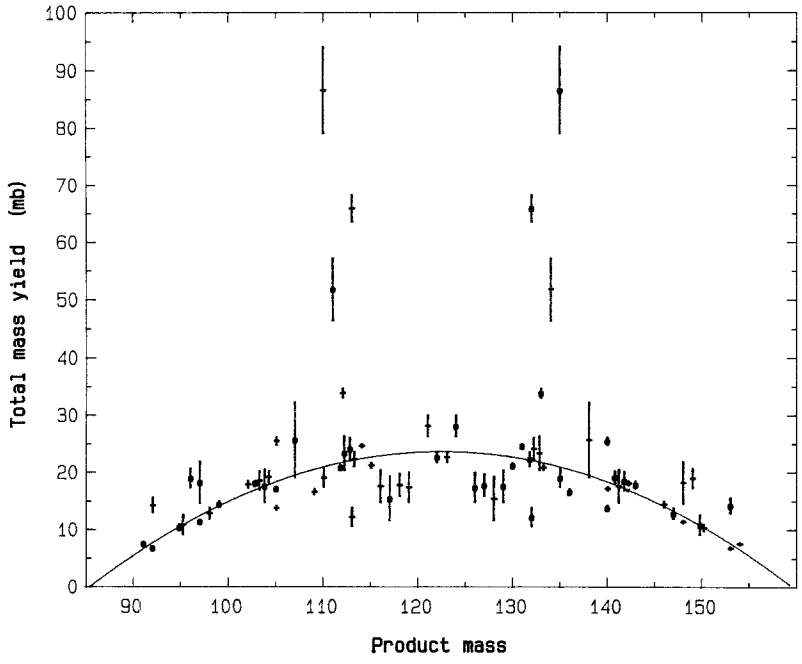

Fig. 6. Total mass yields, σ_A, extrapolated from the measured product yields as described in the text, using $S=0.95$. The circles show the original values, the crosses show the same points reflected about $A_{\text{prod}}=122.5$. The curve is the best fitted parabola

(1).) Note that in this calculation only integer charges were used, although the underlying probability distribution treats charge as a continuous variable. Non-integer masses were, however, used in the calculation of Z_p; strictly speaking these should be interpreted as averages over the two adjacent masses, but this would not alter the results of the calculation.

Values of σ_A were extracted in this way for all the detected products listed in Table 1, and the effect of varying the charge dispersion standard deviation S was investigated; the best value of S was taken as that value which gave the smallest scatter in the resulting plot of σ_A versus A_{prod} consistent with the necessary symmetry $\sigma_A(A_{\text{prod}}) = \sigma_A(A_{cn}-A_{\text{prod}}-\nu)$. Figure 6 shows the mass yields obtained using $S=0.95$, which appears to be roughly optimal. Each point has been plotted twice, at A_{prod} and at the complementary mass $245-A_{\text{prod}}$. The points are considerably scattered, more than expected from the quoted uncertainties (which take no account of the uncertainty in extrapolating from σ_t to σ_A), but the form of the yield curve is basically as expected, an approximate parabola centered at mass 122.5.

A value of $S=0.95$ corresponding to a mass dispersion FWHM of 5.5 u, is slightly larger than expected but not unreasonable, and is used henceforth in this paper. We did not find it necessary to alter the value of $\nu=9$ obtained from the data of Hinde et al. [15].

It may be noted that fitting a parabola centred at mass 122.5 to the points of Fig. 6 leads to an estimate for the total fission cross-section of 590 mb which is in good agreement with the work of Viola and Sikkeland [1], which suggests a total fission cross-section of 610 mb at this incident energy. (The best fit parabola is marked in Fig. 6; clearly the scatter of the points is significantly greater than implied by their nominal uncertainties, suggesting that the uncertainty in the fitted area is realistically about 10%; it should also be remembered that there is an overall uncertainty of 7% in the experimental normalisation.)

B. Fission energy

Since the momenta of the two fragments following scission must be equal and opposite in the moving frame of the fissioning nucleus, in terms of the velocity V_f of the fragment A_f, the total kinetic energy released is

$$E_k=\tfrac{1}{2}A_f V_f^2 \frac{A_{cn}-\nu_{\text{pre}}}{A_{cn}-A_f-\nu_{\text{pre}}}.$$

Now since evaporation of neutrons from the emitted fragment does not alter the average value of its velocity, the experimental estimate V_{cf} of the fission velocity of an observed product provides a measure of the velocity of its parent fragment. Hence, using the relation between A_{prod} and A_f given in the previous section, the best experimental estimate of E_k is $\tfrac{1}{2}A_{\text{prod}}V_{cf}^2\cdot\frac{A_{cn}-\nu_{\text{pre}}}{A_{cn}-A_{\text{prod}}-\nu}$. The values for E_k obtained in this way are listed in Table 2 and plotted in Fig. 7. A correction has been applied to the values arising from cumulative products to account for the fact that the average nuclear charge $\langle Z\rangle$ of the recoiling products (calculated using the charge dispersion approach of the previous section) was lower than that of the final detected product which had been used as the basis of the range/energy conversion for determining V_{cf}; the effect of this correction is to lower the energies deduced for cumulative products by up to 4%, depending on the value of $\langle Z\rangle - Z_{\text{prod}}$.

Although there is significant variation between products, the values of E_k obtained appear to be in overall

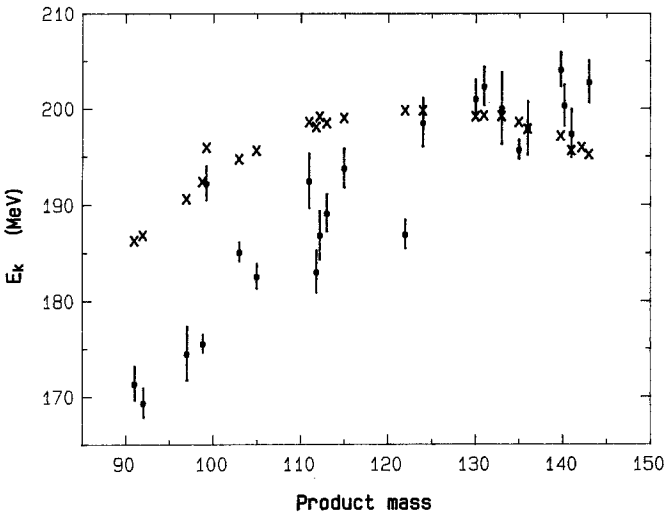

Fig. 7. Experimental estimates of the total kinetic energy release in fission, derived as described in the text, for the 23 products for which recoil distributions were measured. The crosses denote the values of E_{Coul}, the Coulomb energy at 18 fm

reasonable agreement with the value of 195.0 MeV predicted by the most recent formula of Viola et al. [18] for the average total kinetic energy release in fission of ^{254}Fm, and the average TKE measured by Viola et al. [19] of 196 ± 3 MeV.

The simplest approach to modelling the fission energy is as the repulsive Coulomb energy, E_{Coul}, of the two fragments, assuming that at some mutual separation distance, D, the two fragments can be considered essentially at rest but beyond the range of the nuclear forces. The crosses in Fig. 7 show the values calculated using $D = 18$ fm for each fission product for which we have an experimental value; these values are also listed in Table 2. For independent products, E_{Coul} was simply calculated as $\frac{Z_{\text{prod}}(Z_{cn} - Z_{\text{prod}})e^2}{D}$, while for cumulative nuclides the value listed is the properly weighted average of the individual values of E_{Coul} for products populating this nuclide (see the previous section).

The value of $D = 18$ fm was chosen to reproduce the average E_k for all fissions. This value of D leads to predictions of E_k in individual fission events ranging from 186 MeV for $Z_{\text{prod}} = 37$ to 200 MeV for symmetric fission. It can be seen that the experimentally deduced values of E_k agree in all cases with the predicted values to within 10%. However, the data show a systematic trend which is not reproduced by the model. The experimental values show an almost monotonic increase with A_{prod}, whereas the calculated values are approximately symmetric with respect to $A_{\text{prod}} = 122.5$ (symmetric fission). As a result, the calculation systematically overestimates the E_k values for the lighter products and underestimates them for the heavy products.

Note that use of the form $D = d_0(A_f^{1/3} + (A_{cn} - \nu_{\text{pre}} - A_f)^{1/3})$, rather than the constant scission distance of 18 Fm, would increase the calculated Coulomb energy for the most asymmetric products seen by approximately 1% relative to that calculated for symmetric fission, thus slightly exacerbating the observed discrepancy with the experimental E_k values for light products.

Naively, one might expect all the values to show perfect symmetry about $A_{\text{prod}} = 122.5$, since for every light product a complementary heavy fragment must be emitted. However, this need not be the case because the observed products sample different parts of the charge dispersion curve. In general, we observed cumulative products which sample predominantly the more neutron-excessive half of the charge dispersion for the detected fragment (and the less neutron-excessive half for the complementary fragment); accordingly the observed asymmetry in E_k values could qualitatively be explained if fissions in which the light fragment receives larger Z than its most probable value were to result in increased E_k.

This effect actually appears in the Coulomb energy calculation, since the repulsive energy is increased by making the charges of the two fragments more nearly equal. This accounts for the asymmetry of the calculated values in Fig. 7. In particular, note that the calculation predicts an anomalously large E_k value for the independent product ^{99}Tc (which has a Z more than 2 units of charge greater than the most probable Z for its mass), in agreement with the data. In general, however, the Coulomb energy calculation appears to underestimate the observed effect.

Qualitatively, it may be possible to understand this effect as a consequence of changing binding energies of the fragments. Since the most probable fragments lie on the neutron excessive side of the valley of stability, moving along the charge dispersion curve so that the light fragment becomes even more neutron-excessive (and the heavy fragment correspondingly less neutron-excessive) decreases the binding energy of the light fragment while increasing the binding energy of the heavy fragment; since the valley of stability is steeper for the light fragment than for the heavy, the overall effect is to decrease the binding energy of the system, reducing the available energy. It is possible that this then results in the observed reduction of the total kinetic energy released. However, quantitatively, the magnitude of the observed effect seems to be larger than expected from this treatment. It is also possible that E_k may be affected by the angular momentum present, as mentioned below.

C. *Angular anisotropies*

In Fig. 8, the experimental values of the anisotropy, $\omega = P(0°)/P(90°)$, are plotted as a function of product mass. The average of these values (making no allowance for the difference in yields between products) is 1.82. This may be compared to the values measured by Back et al. [20] for the anisotropy averaged over all fission products of 1.92 at 90 MeV and 2.24 at 110 MeV.

The variation in the observed values, up to $\pm 20\%$, is significantly larger than the experimental uncertainties, and apparently represents a genuine difference between products. Since the complete fusion process populates the compound nucleus with a continuous range of angu-

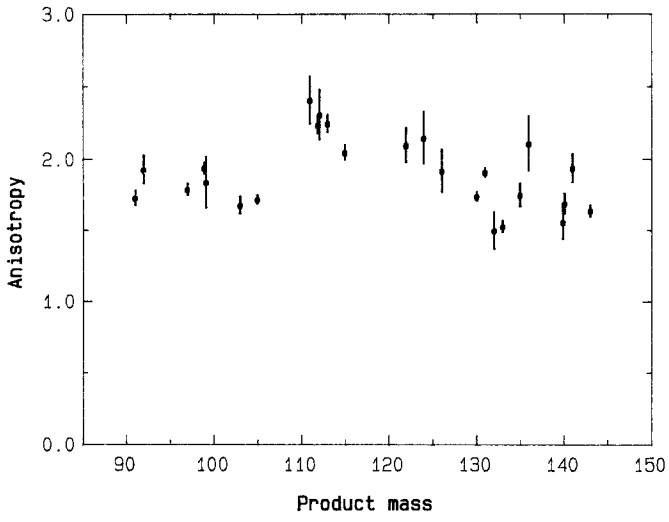

Fig. 8. The anisotropy $\omega = \frac{P(0°)}{P(90°)}$ of the center of mass angular distributions deduced from the measured angular distributions

lar momenta up to the maximum value of 35 $\hbar$, (equivalent to a fission cross-section of 610 mb) and the anisotropy is directly related to the angular momentum of the fissioning system, it would not be surprising if different products sampled different parts of the angular momentum distribution and were accordingly emitted with different average anisotropies.

However, we have not been able to deduce any simple correlation between the nature of the observed product and the value of its anisotropy, and it seems likely that several effects are interacting to produce the experimental anisotropy. One effect which seems to be present is that products from relatively symmetric fissions have larger average anisotropies than those from highly asymmetric fission; this can be understood if an increase in the angular momentum of the fissioning system increases the probability of symmetric fission relative to asymmetric fission, so that the average angular momentum involved in forming near-symmetric products is larger than in forming asymmetric products. (This might also account for the fact that the anisotropy measured in on-line experiments [20] is apparently somewhat larger than our average value, since yields of near symmetric products are larger than asymmetric yields). However, data for a number of products conflict with this overall trend. There is also some indication of a negative correlation between E_k and ω, so that products for which the experimental value of E_k was larger than expected from the Coulomb model have smaller than average values of ω; again several of the data conflict with this approach. Such a correlation is perhaps not surprising, in that the effect of increased angular momentum could be to increase the scission distance, D, and hence lower the Coulomb repulsion between the two fragments at scission. In the absence of a full theoretical treatment of the expected variation of ω for individual products, it appears that the data are not sufficiently complete to isolate all of the effects which are present, but they certainly indicate significant variations, which have not previously been observed or predicted.

V. Conclusions

This study has demonstrated the ability of recoil measurements of this type to make precise determinations of the kinematic properties of individual products from fission. The precision of the angular distribution measurement was poorer than that of the range measurement, but the resulting values of the recoil velocity of the fissioning system were generally determined to within 10% and (with two exceptions) were all consistent with the theoretical value, v_{cn}, for complete fusion. Working with the range measurement alone, and accepting that the reaction mechanism is complete fusion, enables the values of the fission energy to be determined generally to better than 1%, and the correlations observed in the data at this level indicate that this uncertainty is reasonably realistic. The absolute values deduced for the fission energy E_k are entirely consistent with the average value expected from systematics, indicating that the magnitude of any systematic errors (such as errors in the range/energy relations used) are very small. It therefore appears that such studies can play an extremely powerful role in further studies of fission.

It has been confirmed that the reaction mechanism for 101 MeV ^{16}O on ^{236}U is essentially entirely complete fusion, with fission of the nucleus resulting after emission of some neutrons from the ^{254}Fm compound nucleus. The measured yields of 38 products can be reasonably explained using the UCD hypothesis with a charge dispersion whose standard deviation is 0.95 charge units, assuming a total neutron multiplicity of 9, of which 2.5 neutrons are emitted prior to scission, as suggested by neutron measurements on similar systems [15]. The mass yield curve then appears to be roughly parabolic, with a total fission cross-section of approximately 590 mb, in good agreement with the results of on-line measurements [1].

The present study revealed significant variations between individual products in the values of the kinetic energy release, E_k, and the angular anisotropy, ω, which have not previously been reported or predicted. The E_k show a systematic variation apparently related to the deviation of the charge split in a given fission event from the most probable division predicted by UCD, so that charge splits closer to equality lead to enhanced E_k (by 10–15 MeV per charge unit). This effect is significantly greater than expected from changes in the Coulomb repulsion assuming fission to occur at a constant separation distance, but may be understandable in terms of changes in the binding energy of the system. The angular anisotropies also show significant variations, suggesting that different angular momentum states of the compound system preferentially populate different products, but the relationship appears to be complex; symmetric fission products generally have larger anisotropies than products from asymmetric fission, but there also seems to be some correlation between E_k and ω – large E_k

is often associated with small ω. These effects merit further study.

This work was made possible by grants from the North Atlantic Treaty Organisation and the Natural Sciences and Engineering Research Council of Canada. Work described in this paper was undertaken as part of the Underlying Research Programme of the United Kingdom Atomic Energy Authority. Preliminary sorting and analysis of the decay data was performed by A. Bruccoleri and A. Wolf, McGill Chemistry Department and S. Montague, Nuclear Physics and Instrumentation Division, Harwell. Targets and catcher foils were prepared by M. Miller, NPID, Harwell.

References

1. Viola, V.E. Jr., Sikkeland, T.: Phys. Rev. **128**, 767 (1962)
2. Sikkeland, T., Haines, E., Viola, V.E. Jr.: Phys. Rev. **125**, 1350 (1962)
3. Lee, C.H., Yu, Y.W., Lee, D., Kudo, H., Moody, K.J., Seaborg, G.T.: Phys. Rev. C**38**, 1757 (1988)
4. Yu, Y.W., Lee, C.H., Moody, K.J., Kudo, H., Lee, D., Seaborg, G.T.: Phys. Rev. C**36**, 2396 (1987)
5. Alexander, J.M.: In: Nuclear chemistry. Yaffe, L. (ed.), Chap. 4. New York: Academic 1968
6. Tserruya, I., Steiner, V., Fraenkel, Z., Jacobs, P., Kovar, D.G., Henning, W., Vineyard, M.F., Glagola, B.G.: Phys. Rev. Lett. **60**, 14 (1988)
7. Goodall, J.-A.B.: UKAEA, Rept. No. AERE-M3185 1981 (unpublished)
8. Reus, U., Westmeier, W., Warnecke, I.: At. Nucl. Data Tables **29**, 1 (1983)
9. Parker, D.J., Asher, J., Conlon, T.W., Naqib, I.: Phys. Rev. C**30**, 143 (1984)
10. Parker, D.J., Hogan J.J., Asher, J.: Phys. Rev. C**35**, 161 (1987)
11. Northcliffe, L.C., Schilling, R.F.: Nucl. Data Tables A**7**, 233 (1970)
12. Friedlander, G.: Proceedings of the Symposium on Physics and Chemistry of Fission, Vol. 2, p. 265. Wien: IAEA 1965 and many references compiled therein
13. Freiesleben, H., Kratz, J.V.: Phys. Rep. **106**, 1 (1984)
14. Hinde, D.J., Charity, R.J., Foote, G.S., Leight, J.R., Newton, J.O., Ogaza, S., Chattejee, A.: Nucl. Phys. A**452**, 550 (1986)
15. Hinde, D.J., Leigh, J.R., Bokhorst, J.J.M., Newton, J.O., Walsh, R.L., Boldeman, J.W.: Nucl. Phys. A**472**, 318 (1987)
16. Goeckerman, R.H., Perlman, I.: Phys. Rev. **76**, 628 (1949)
17. Lutzenkirchen, K., Kratz, J.V., Bruchle, W., Gaggeler, H., Summerer, K., Wirth, G.: Z. Phys. A – Atoms and Nuclei **317**, 55 (1984)
18. Viola, V.E. Jr., Kwiatkowski, K., Walker, M.: Phys. Rev. C**31**, 1550 (1985)
19. Viola, V.E. Jr., Back, B.B., Wolf, K.L., Awes, T.C., Gelbke, C.K., Breuer, H.: Phys. Rev. C**26**, 178 (1982)
20. Back, B.B., Betts, R.R., Gindler, J.E., Wilkins, B.D., Saini, S., Tsang, M.B., Gelbke, C.K., Lynch, W.G., McMahon, M.A., Baisden, P.A.: Phys. Rev. C**32**, 195 (1985)

D.J. Parker, J. Asher
Nuclear Physics and Instrumentation Division
Harwell Laboratory
Oxfordshire OXII ORA
UK

J.J. Hogan
Department of Chemistry
McGill University
Montreal
Quebec
Canada H3A 2K6